A Spray Interaction Model with Application to Surface Film Wetting

K. V. Meredith*, X. Zhou
Research Division, FM Global, USA
karl.meredith@fmglobal.com and xiangyang.zhou@fmglobal.com
A. Heather
OpenCFD Ltd., UK
a.heather@opencfd.co.uk

Abstract

In a fire suppression environment, sprinkler spray wets solid surfaces via droplet impingement. A framework for modeling the interaction of sprays with solid surfaces, with the intention of simulating fire suppression, has been developed. The spray interaction model includes impingement, splashing, and subsequent liquid-film transport over solid surfaces. The thin film-transport equations for mass continuity, momentum, and energy form the basis for the spray-film interaction model. The model has been implemented in OpenFOAM®† and subsequently coupled with a fire growth model (FireFOAM). Experimental measurements of splashing behavior are shown and used for model validation. Model validation is demonstrated for droplets impinging on wet corrugated cardboard surfaces over a range of Weber numbers. Comparisons include the splashed mass measured as a function of radial distance from the initial impingement location.

Introduction

The basic mechanism for sprinkler-based fire suppression relies on relatively large water droplets (diameters typically on the order of 1 mm[1]) that can penetrate through the fire plume and reach the burning surface. Due to the large diameter and short residence time, little vaporization occurs from the droplet. Thus, for sprinkler-based fire suppression the dominant mechanism contributing to fire suppression of solid based fuels is the interaction of liquid water with the burning solid[2].

In an effort to simulate this fire suppression phenomenon, a computational fluid dynamics (CFD) model, FireFOAM, has been developed in the OpenFOAM[3] framework. FireFOAM incorporates physics-based models for turbulence, combustion[4], soot[5], radiation[6], pyrolysis[7], and sprinkler spray patternation[1]. A water film transport model has been incorporated into the general framework for simulating the interaction of water with solid-fuel pyrolysis.[8]. In this study, the goal is to apply a robust model for spray-surface interaction and validate this model against conditions related to fire suppression, thus moving one step closer to achieving a comprehensive CFD model for simulating fire growth and suppression.

Much work has been done in the area of spray-wall and spray-film interaction. Many of the experimental studies and developed models have applied to liquid fuel sprays in a combustion environment. An excellent review of spray impingement work has been provided by Lee and Ryou[9]. Bai[10], and more recently Bai et al.[11], have proposed a practical spray impingement model based on empirical data and conservation of mass, momentum, and energy. Stochastic behavior is included in the model to mimic the randomness of the post-impingement behavior. Further discussion of this model will be provided below.

The scope of the water-film transport model ranges from when the sprinkler spray impinges on the solid-fuel surface to when the water runs off the surface, vaporizes, absorbs into the fuel, or splashes back into the gas phase. The thin-film assumption, which has been used successfully by a number of authors[12,13], is used in this study, and has been described elsewhere[8,14]. The thin film assumption yields two-dimensional equations for the film height, the wall-tangential components of velocity, and the mean film enthalpy.

The surface film based water-transport model has been previously validated for continuous film flow over inclined surfaces. Results have been shown to match the analytical Nusselt solution for film flow and to match experimental data for velocity and film thickness over a wide range of film Reynolds number[8]. In addition, the partial wetting treatment of the model in the absence of interfacial mass transfer was validated against experimental wetted-area fraction measurements[14]. The validation presented in this study includes the spray-film interaction model including droplet impingement and splashing.

In this study, the film-transport equations are described along with spray interaction source terms. The experimental setup is outlined for verifying splashing behavior. Finally, model validation results are shown.

*Corresponding author: karl.meredith@fmglobal.com

†OpenFOAM®is a registered trademark of the OpenFOAM Foundation.

Table 1. Spray impingement source terms for film-transport conservation equations.

Term	Impingement	Splashing	Equation
Mass	$S_{\rho\delta,imp} = \sum_i \dot{m''}_{imp,i}$	$S_{\rho\delta,splash} = -\sum_i \dot{m''}_{splash,i}$	1
Pressure	$p_{imp} = \sum_i \dot{m''}_{imp,i} (\mathbf{v}_{imp,i} \cdot \mathbf{n})$	$p_{splash} = -\sum_i \dot{m''}_{splash,i} (\mathbf{v}_{splash,i} \cdot \mathbf{n})$	3
Tangential momentum	$\mathbf{S}_{\rho\delta\mathbf{U},imp} = \sum_i \dot{m''}_{imp,i} \mathbf{v}_{imp,t,i}$	$\mathbf{S}_{\rho\delta\mathbf{U},splash} = -\sum_i \dot{m''}_{splash,i} \mathbf{v}_{splash,t,i}$	4
Energy	$S_{\rho\delta h,imp} = \sum_i \dot{m''}_{imp,i} h_{imp,i}$	$S_{\rho\delta h,splash} = -\sum_i \dot{m''}_{splash,i} h_{splash,i}$	5

Surface Film Model

Film Transport Equations

The governing transport equations for film flow are presented here. For simplicity, only those source terms related to spray interaction are shown. The integrated mass continuity equation is defined as

$$\frac{\partial \rho\delta}{\partial t} + \nabla_s \cdot [\rho\delta\mathbf{U}] = S_{\rho\delta,imp} + S_{\rho\delta,spl} \tag{1}$$

where δ is the film thickness, ∇_s is the vector differential operator tangential to the surface, $(\partial/\partial x, \partial/\partial y)^{\mathsf{T}}$. $S_{\rho\delta}$ is the mass source per unit wall area due to impingement $(S_{\rho\delta,imp})$ and splashing $(S_{\rho\delta,spl})$.

The momentum equation, integrated over film thickness, is

$$\frac{\partial \rho\delta\mathbf{U}}{\partial t} + \nabla_s \cdot [\rho\delta\mathbf{U}\mathbf{U}] = -\delta\nabla_s p + \mathbf{S}_{\rho\delta\mathbf{U}} \tag{2}$$

$$p = p_{imp} + p_{splash} \tag{3}$$

$$\mathbf{S}_{\rho\delta\mathbf{U}} = \mathbf{S}_{\rho\delta\mathbf{U},imp} + \mathbf{S}_{\rho\delta\mathbf{U},spl} \tag{4}$$

where $\mathbf{U}$ represents the mean, tangential velocity of the film. The pressure term, p, comprises forces in the wall-normal direction, namely impingement pressure (p_{imp}) and splashing pressure (p_{splash}). $\mathbf{S}_{\rho\delta\mathbf{U}}$ includes the momentum source per unit wall area due to impingement $(\mathbf{S}_{\rho\delta\mathbf{U},imp})$ and splashing $(\mathbf{S}_{\rho\delta\mathbf{U},spl})$

The enthalpy form of the film energy transport equation is represented as

$$\frac{\partial \rho\delta h}{\partial t} + \nabla_s \cdot [\rho\delta\mathbf{U}h] = S_{\rho\delta h,imp} + S_{\rho\delta h,spl} \tag{5}$$

where the film is represented by a mean enthalpy, h resulting in a mean film temperature, T_f. Energy interactions with spray impingement and splashing are captured as $S_{\rho\delta h,imp}$ and $S_{\rho\delta h,spl}$.

The transport equations for the water-film model have been implemented in OpenFOAM. The film model is solved on a 2-D surface mesh that is discretized in both directions tangential to the surface, but is only one cell thick in the direction normal to the surface. The surface mesh is extruded from the boundary mesh of the larger, gas-phase domain. This approach simplifies the implementation by separating the gas-phase physics from the water transport physics and localizes the communication between the regions to maintain a modular design.

Spray-Interaction Source terms

Source terms required for the film-transport equations are shown in Table 1, where $\dot{m''}_{imp,i}$ is the mass flux of the i^{th} impinging droplet. The amount of mass impinging on any given surface is computed via interfacing with the Lagrangian particle tracking in the gas phase. Additionally, $\mathbf{n}$ is the surface normal vector, $\mathbf{v}_{imp,i}$ is the velocity, $\mathbf{v}_{imp,t,i}$ is the surface-tangential droplet velocity vector. The splashing source terms carry similar definitions.

Impingement Submodel

Complex interactions occur when spray impacts on a boundary surface. The result of such an impact can range from adhesion, bouncing, and splashing. Bouncing means the impinging droplet wholly recoils off of the

Table 2. Values of critical Weber number for transition between impingement behavior.

Regime	Criterion
Adhesion	$\mathrm{We} \lesssim 1$
Bounce	$1 \lesssim \mathrm{We} \lesssim 20$
Adhesion	$20 \lesssim \mathrm{We} \lesssim \Lambda_{wet} \cdot \mathrm{La}^{-0.183}$
Splash	$\Lambda_{wet} \cdot \mathrm{La}^{-0.183} \lesssim \mathrm{We}$

surface, remaining intact. Splashing occurs when the impinging droplet impacts the surface and breaks into smaller, secondary droplets that leave the surface. Some of the incident droplet's kinetic energy is transferred into the secondary droplets. Splashing (and to a lesser extent bouncing) influences the amount of impinging mass that remains on the solid surface. The effects of splashing can be quite pronounced when considering fire suppression because splashing can result in a reduced amount of water remaining on solid fuel surfaces. The model for droplet interaction with the boundary surface is taken from Bai [12] and Bai et al. [11], with slight modification for application to splashing on wetted corrugated cardboard surfaces. In the following discussion, only aspects of the model related to impingement on wet surfaces are considered. Impingement on dry surfaces, although an interesting topic for investigation, is not part of the current scope and is expected to have minimal impact in fire suppression. The vast majority of droplet impingement will occur on previously wetted surfaces.

Much of the behavior of impinging droplets can be characterized by the Weber number. The droplet Weber number (We), representing the ratio of inertial to surface tension forces, is given as

$$\mathrm{We} = \rho V_{I,n}^2 d_I / \sigma \tag{6}$$

where $V_{I,n}$ is the surface-normal incident velocity of the impinging droplet. For $\mathrm{We} < \mathrm{We_c}$, a droplet will adhere to the dry wall. For $\mathrm{We} > \mathrm{We_c}$ the droplet impingement will result in a splash.

Also, spray impingement behavior depends largely on the wall surface characteristics. Different behavior is observed for a dry wall compared to a wetted wall. A cut-off parameter is used in the model to determine when the wall is classified as 'wet'. This parameter, δ_{wet}, has been experimentally observed to be ~ 0.5 mm for corrugated cardboard. For a wetted wall (i.e. $\delta > \delta_{wet}$), several regimes of spray impingement have been observed, and these are shown in Table 2. At low We, adhesion and bouncing occur, followed by splashing. Bouncing differs from splashing in that the whole mass of the impinging droplet is rebounded off the solid boundary as a complete, intact droplet. Bouncing, while included in the computational model for completeness, will not be discussed here as $\mathrm{We_c}$ for bounce is much lower than the range of interest for fire suppression environments. Table 2 lists the various transitions for the different regimes. The value of Λ_{wet} represents the roughness of the surface.

La is the droplet Laplace number, and denotes the ratio of surface tension force to viscous force in the droplet,

$$\mathrm{La} = \rho \sigma d_I / \mu^2 \tag{7}$$

where ρ is the liquid density, σ is the surface tension, d_I is the impinging droplet diameter, and μ is the liquid viscosity.

Adhesion In the adhesion regime, the entire incident droplet mass is deposited on the wall. The normal component of the droplet kinetic energy is converted to an impingement pressure, and the tangential momentum increases the local film tangential momentum, as was previously shown in in Table 1.

Splash In the splashing regime, each incident droplet produces N_p secondary parcels. A parcel is a grouping of individual droplets with identical properties, including diameter, velocity, etc. Each secondary parcel contains a mass of m_S/N_p where m_S is the total mass of secondary droplets. A value of $N_p = 2$ was shown by Bai et al. [11] to be a reasonable assumption. The diameters of secondary droplets are found from a χ^2 distribution function

$$f(d) = \frac{1}{\overline{d}} \exp\left(-\frac{d}{\overline{d}}\right) \tag{8}$$

where $\overline{d}$ is the number mean diameter. The number mean diameter is related to the volumetric mean diameter as

$$\overline{d} = \frac{d_V}{6^{1/3}} = \frac{1}{6^{1/3}} \left(\frac{r_m}{N_S}\right)^{1/3} d_I \tag{9}$$

where d_I is the incident droplet diameter, r_m is the ratio of splashing mass (m_S) to incident mass (m_I), and N_S is the total number of secondary droplets resulting from a splash. The mass ratio, r_m, is taken to be

$$r_m = \frac{m_S}{m_I} = \begin{cases} \beta_{dry,min} + \omega(\beta_{dry,max} - \beta_{dry,min}), \text{ for dry wall} \\ \beta_{wet,min} + \omega(\beta_{wet,max} - \beta_{wet,min}), \text{ for wet wall} \end{cases} \tag{10}$$

where ω is a random number* chosen from a uniform distribution between $(0, 1)$, and the β parameters represent respective minimum and maximum values of the mass ratio. For the wet wall, values of r_m can be larger than 1 because splashing may entrain liquid from the liquid film. The total number of secondary droplets derived from a splash is given as

$$N_S = a_0 \left(\frac{\mathrm{We}}{\mathrm{We_c}} - 1 \right) \tag{11}$$

where a_0 is a correlation parameter, and $\mathrm{We_c}$ is the critical Weber number for splashing. The cumulative distribution function of Equation 8 is used to determine the sizes of the N_p secondary droplets, d_i $(i = 1...N_p)$ by taking N_p random samples, each with a probability γ_i $(0 < \gamma_i < 1)$. Now, knowing the secondary droplet diameters, d_i, the number of droplets n_i in each secondary parcel i is found from mass conservation. The amount of splashed mass is divided into N_p equal parcels, and the number of droplets in each parcel is found from the following expression:

$$n_i d_i^3 = \frac{r_m d_I^3}{N_p} \tag{12}$$

The velocity vector of the splashed droplets is

$$\mathbf{V}_S = \mathbf{V}_{S,t} + \mathbf{V}_{S,n} \tag{13}$$

$\mathbf{V}_{S,t}$ and $\mathbf{V}_{S,n}$ (splash tangential and normal components) are dependent on the incident velocity tangential, $\mathbf{V}_{I,t}$, and normal, $\mathbf{V}_{I,n}$, components, respectively. $\mathbf{V}_{S,t}$ comes wholly from $\mathbf{V}_{I,t}$ and $\mathbf{V}_{S,n}$ is derived from $\mathbf{V}_{I,n}$. However, contrary to intuition, the resulting $\mathbf{V}_{S,n}$ will generally not be normal to the surface.

$\mathbf{V}_{S,t}$ is defined as

$$\mathbf{V}_{S,t} = C_f \mathbf{V}_{I,t} \tag{14}$$

where C_f designates a friction coefficient typically in the range of $(0.6, 0.8)$.

For the velocity vector $\mathbf{V}_{S,n,i}$ (again, this velocity vector is not normal to the surface, but only derived from the incident normal velocity) three quantities are needed. First, the azimuthal angle $\phi_{S,i}$ is randomly sampled from the range $(0, 2\pi)$. The ejection angle $\theta_{S,i}$, originally proposed to be randomly sampled from $(40°, 85°)$ [11] with respect to the surface normal, seems to follow more closely a normal distribution, as will be discussed later. Thus, $\theta_{S,i}$ is set to be randomly sampled from a normal distribution with a mean of $\theta_{S,i,mean}$ and a standard deviation of $\theta_{S,i,mean,std}$. The orientation of the surface only plays a role in determining the prior trajectory of the incoming droplet and the subsequent trajectory of the splashed droplets. The velocity magnitude $V_{S,n,i}$ is derived from energy conservation:

$$\frac{1}{2}\frac{m_S}{N_p}\left[(V_{S,n,1})^2 + ... + (V_{S,n,N_p})^2\right] = E_{K,S} \tag{15}$$

$E_{K,S}$ is the amount of kinetic energy available for the splash event due to $\mathbf{V}_{I,n}$ only, assuming that the kinetic energy that causes splashing is the surface-normal kinetic energy.

$$E_{K,S} = E_{K,I} + E_{\sigma,I} - E_D - E_{\sigma,S} \tag{16}$$

The incident kinetic energy is defined as $E_{K,I} = \frac{1}{2} m_I V_{I,n}^2$. $E_{\sigma,I}$ is the surface energy of incident droplets and $E_{\sigma,S}$ is the surface energy of secondary droplets. The dissipative energy loss, E_D, is specified as

$$E_D = \max\left(C_{E_K,I} E_{K,I}, C_{E_D} \mathrm{We_c} \pi \sigma d_I^2\right) \tag{17}$$

*Due to the nature of random number generators, if the random number generator uses the same seed then the result is reproducible. Thus, a simulation performed with the same seed will produce the same results.

where $\mathrm{We_c}$ is the splashing critical Weber number and $C_{E_{K,I}}$ and C_{E_D} are model parameters for specifying the amount of incident kinetic energy that is dissipated.

If $N_p = 1$, then Equations 15 to 17 are sufficient to determine $V_{S,n,i}$. If $N_p > 1$, then a size-velocity correlation is used:

$$\left(\frac{V_{S,n,1}}{V_{S,n,i}}\right) \approx ln\left(\frac{d_1}{d_I}\right) / ln\left(\frac{d_i}{d_I}\right) \quad (i = 2...N_p) \tag{18}$$

Equation 18 is substituted into Equation 15 to give $V_{S,n,1}$. Then, $V_{S,n,1}$ is substituted into Equation 18 to obtain the remaining $V_{S,n,i}$ $(i = 2...N_p)$.

Experimental Methods

Figure 1 shows the experimental setup for measuring the splashing mass fraction. Details of the experimental measurements have been reported elsewhere [15], and only a brief overview will be provided here. The liquid droplets were generated using a syringe pump that was controlled to dispense the liquid at a steady rate of 100 ml/hr. The droplet was formed at the tip of the needle and detached under its own weight. The droplet size was changed by using different needles. The height of the needle above the surface was adjusted to change the droplet impinging velocity. The cardboard sample was placed in the center of a pan and a cover plate. There is gap of about 4 mm between the sample and the cover plate. When a falling droplet impinges on the cardboard surface, the splashed liquid is collected by the plate, and the deposited liquid is collected by the cardboard and the pan. A precision weighing balance with a capacity of 210 g and a standard deviation of 0.1 mg was used to measure the mass difference. An image of the splashing event captured 15 ms after impact is shown in Figure 2 for $\mathrm{We} = 810$.

The PMMA cover plate shown in Figure 1 was divided into five annular zones with six radii of 22, 40, 60, 89, 134 and 190 mm. The first annulus near the impingement center is in the radial range from 22 to 40 mm, and the fifth annulus is from 134 to 190 mm. After successive droplets impinged continuously on the cardboard surface, the droplets splashed in each annulus were collected carefully using a paper tissue. The mass of splashed droplets in each annulus was then measured as the mass difference of the paper tissue, and was expressed as the mass fraction relative to the impact droplets. A laser-based Shadow-Imaging system was used in this work to measure droplet size and velocity. [16]

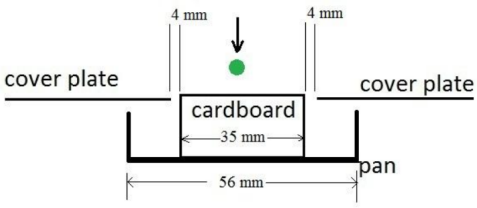

Figure 1. A sketch of the experimental setup to measure the splashing mass fraction.

Figure 2. The splashing event captured at 15 ms after impact for $\mathrm{We} = 810$.

Extension of Splashing Model to Corrugated Cardboard

The input parameters to the spray impingement model were obtained via optimization against the measured splashed radial distribution. Due to the large difference in behavior of the low We splashing versus the high We splashing, many of the parameters were optimized as a function of We. The values of We used in the optimization were 340 and 810. Experimental measurements at the intermediate $\mathrm{We} = 570$ were not used in the optimization. Instead, input parameters for this We were found via linear interpolation. Table 3 shows the splash model parameters as a function of We.

For optimization, the Multiple Objective Genetic Algorithm (MOGA) algorithm provided by the Dakota [17] optimization software was used. The MOGA package allows multi-objective optimization without the need to specify weights on the various objective function values. For the splashing optimization, two objective functions were chosen. The first was the sum of least squares difference between the predicted radial splashed mass distribution and the measured distribution for $\mathrm{We} = 340$. The second objective function was similar, only for $\mathrm{We} = 810$.

Table 3. Input parameters and empirical constants for Bai splashing model.

Parameter	Original proposed value[11]	Optimized value We = 340	Interpolated Value We = 570	Optimized Value We = 810	Equation No.
δ_{wet} (mm)	—	0.0005	0.0005	0.0005	
Λ_{wet}	1320	3274	3274	3274	Table 2
C_f	0.6-0.8	0.7	0.7	0.7	14
$\beta_{wet,min}$	0.2	0.0368	0.209	0.374	10
$\beta_{wet,max}$	1.1	1.284	1.323	1.359	10
$\theta_{S,i,wet,mean}$	—	56.8	38.4	20.8	
$\theta_{S,i,wet,std}$	—	23.8	23.8	23.8	
$C_{E_{K,I}}$	0.8	0.956	0.672	0.400	17
C_{E_D}	0.0833	0.0625	0.0625	0.0625	17
a_0	5.0	13.72	22.37	30.63	11

Results and Discussion

The spray-impingement model was tested by simulating the experimental setup described above. Fifty drops of water, 4.37 mm in diameter, were dropped consecutively onto the center of the cardboard sample. Comparisons between the predicted and measured radial splash fractions are shown in Figure 3 for three values of We. For We $= 340$, very little splashing occurs, and the model does reasonably well in predicting this behavior. At higher values of We, more and more of the impinging mass ends up being splashed outward radially.

While details in the splashed mass distribution are not captured in the model exactly, the model performs relatively well in predicting the overall behavior. Figure 4 shows the total fraction of splashed beyond the 0-22 mm range for all three We. As We increases from 340 to 570, the splashed fraction increases nearly three-fold. A subsequent increase from 570 to 810 the splashed fraction increases by only a few percentage points, suggesting a limiting value for the splash fraction at high We. The simulation captures this trend nicely.

As previously mentioned, the values for $\theta_{S,i}$ were measured experimentally for We $= 810$ at $t = 5ms$ and $t = 15ms$ after the impingement time, and a pdf of the measured values is shown in Figure 5. The majority of the measured angles are between $30 - 60°$. Also shown in Figure 5 is the pdf of the angles resulting from the optimization simulations, obtained from the optimized normal distribution. The optimized distribution yields angles that are less than the measured values. This likely stems from inadequacies in the model to capture enough detail of the actual splashing process.

The diameters of secondary droplets were also measured experimentally at We $= 810$ at $t = 5ms$ and $t = 15ms$ after the impingement time, and a pdf of the measured values is shown in Figure 6. The minimum and maximum diameter values for the splash model were set based on the experimentally observed values. The number mean of the distribution is mainly a function of r_m and a_0. Also shown in Figure 6 are the values for d_{v50}, representing the volume-median droplet diameter (i.e., 50% of the cumulative water volume is represented by droplets having a diameter smaller than d_{v50}).

Comparisons of splashed velocity and diameter of secondary droplets created from a splash event were made with experimental data. Figure 7 shows a comparison of the normalized secondary droplet velocity, $V_s/V_{I,n}$, and normalized secondary droplet diameter, d_s/d_I, with experimental data. Here, $V_{I,n}$ represents the surface-normal component of the primary droplet, and d_I represents the primary droplet diameter. The comparison to experimental data falls within the scatter of the measured values at low d_s/d_I, and over predicts the experimentally measured velocities at the high d_s/d_I range. The main drivers in the model for determining the predicted secondary velocities are Eq. 18, $C_{E_{K,I}}$, and C_{E_D}.

Summary and Conclusions

The current validation of the model for spray-impingement, consisting of adhesion and splashing, is a key milestone in achieving a fully validated model for use in fire suppression simulations. The model of Bai et al.[11] has been extended for use in simulating spray impingement on corrugated cardboard surfaces in the range of We applicable to fire suppression scenarios. Changes to the original model include defining a separate range of $\theta_{S,i}$ angles to be sampled from for dry and wet surfaces, based on experimental observation. Additionally, empirical model constants have been optimized to give a good match with experimentally measured radial splashed mass

distributions for a range of We.

Acknowledgments

This work was funded by FM Global under the Strategic Research Programs for Fire Modeling and Sprinkler Technology. The authors appreciate Yi Wang and Yibing Xin for their suggestions regarding the modeling and experimental work.

References

[1] N. Ren, H. R. Baum, and A. W. Marshall. A comprehensive methodology for characterizing sprinkler sprays. *Proceedings of the Combustion Institute*, 33(2):2547 – 2554, 2011.

[2] V. Novozhilov, B. Moghtaderi, J. H. Kent, and D. F. Fletcher. Solid fire extinguishment by a water spray. *Fire Safety Journal*, 32(2):119 – 135, 1999.

[3] H. G. Weller, G. Tabor, H. Jasak, and C. Fureby. A tensorial approach to computational continuum mechanics using object-oriented techniques. *Computers in Physics of Fluids*, 12(6):620–631, Nov/Dec 1998.

[4] Y. Wang, P. Chatterjee, and J. L. de Ris. Large eddy simulation of fire plumes. *Proceedings of the Combustion Institute*, 33(2):2473–2480, 2011. doi:10.1016/j.proci.2010.07.031.

[5] P. Chatterjee, J. L. de Ris, Y. Wang, and S. B. Dorofeev. A model for soot radiation in buoyant diffusion flames. *Proceedings of the Combustion Institute*, 33(2):2665–2671, 2011. doi:10.1016/ j.proci.2010.06.112.

[6] P. Chatterjee, N. Krishnamoorthy, Y. Wang, J. L. de Ris, and S. B. Dorofeev. CFD simulation of radiative heat transfer between a buoyant turbulent fire and inert parallel panels. *Proceedings of the 12th Fire Science and Engineering Conference, INTERFLAM, Nottingham, UK*, pages 777–788, Jul 5-7, 2010.

[7] N. Krishnamoorthy, M. Chaos, M. M. Khan, P. Chatterjee, Y. Wang, and S. B. Dorofeev. Application of bench-scale material flammability data to model flame spread in medium- scale parallel panel test. *Proceedings of the 12th Fire Science and Engineering Conference, INTERFLAM, Nottingham, UK*, pages 709–720, Jul 5-7, 2010.

[8] K. V. Meredith, Y. B. Xin, and J. de Vries. A numerical model for simulation of thin-film water transport over solid fuel surfaces. *Fire Safety Science*, pages 415–428, 2011.

[9] S. H. Lee and H. S. Ryou. Development of a new spray/wall interaction model. *International Journal of Multiphase Flow*, 26(7):1209 – 1234, 2000.

[10] C. X. Bai and A. D. Gosman. Development of methodology for spray impingement simulation. *Society of Automotive Engineers*, (SAE 950283), 1995.

[11] C. X. Bai, H. Rusche, and A. D. Gosman. Modelling of gasoline spray impingement. *Atom. Sprays*, 12:1–27, 2002.

[12] C. X. Bai and A. D. Gosman. Mathematical modeling of wall films formed by impinging sprays. *Society of Automotive Engineers*, (SAE 960626), 1996.

[13] D. W. Stanton and C. J. Rutland. Multi-dimensional modeling of thin liquid films and spray-wall interactions resulting from impinging sprays. *Int. Journal of Heat and Mass Transfer*, 41(20):3037 – 3054, 1998.

[14] K. V. Meredith, A. Heather, J. de Vries, and Y. Xin. A numerical model for partially-wetted flow of thin liquid films. *Computational Methods in Multiphase Flow*, VI:239–250, June 15-17 2011.

[15] X. Zhou. Experimental measurements of a liquid droplet impinging on corrugated cardboard surface. *ICLASS 12th Triennial Int. Conference on Liquid Atomization and Spray Systems, Heidelberg, Germany*, 2012.

[16] X. Zhou and H.-Z. Yu. Experimental investigation of spray formation as affected by sprinkler geometry. *Fire Safety Journal*, 46:140–150, 2011.

[17] B. Adams, W. Bohnhoff, K. Dalbey, J. Eddy, M. Eldred, D. Gay, K. Haskell, P. Hough, and L. Swiler. Dakota, a multilevel parallel object-oriented framework for design optimization, parameter estimation, uncertainty quantification, and sensitivity analysis: Version 5.0 user's manual,. Technical report, Sandia Technical Report SAND2010-2183, December 2009. Updated December 2010 (Version 5.1).

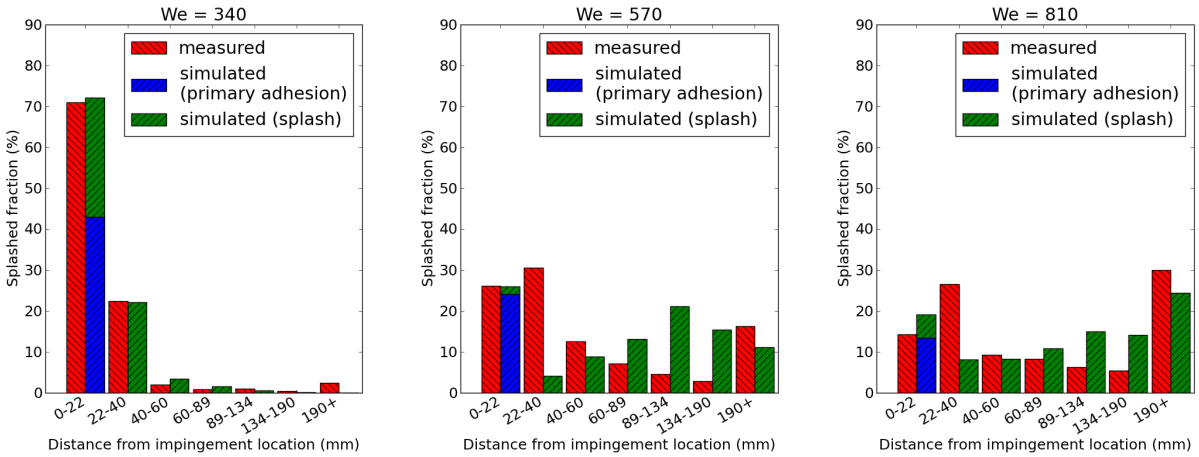

Figure 3. Simulated and measured splashed mass fractions as a function of radial distance from primary droplet impingement location, shown for We = 340, We = 570, We = 810.

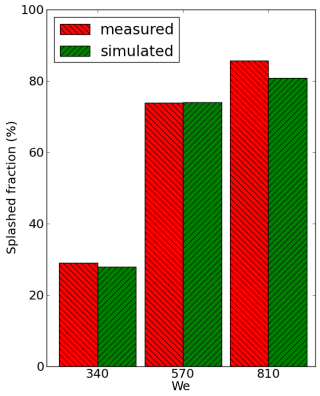

Figure 4. Simulated and measured splashed mass fractions for We = 340, We = 570, We = 810.

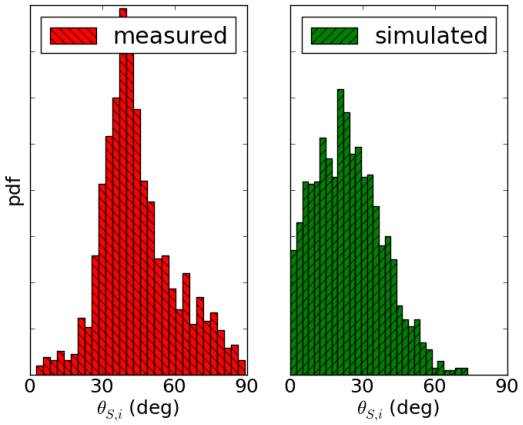

Figure 5. Measured secondary droplet angle based on wet surface droplet impingement at We = 810.

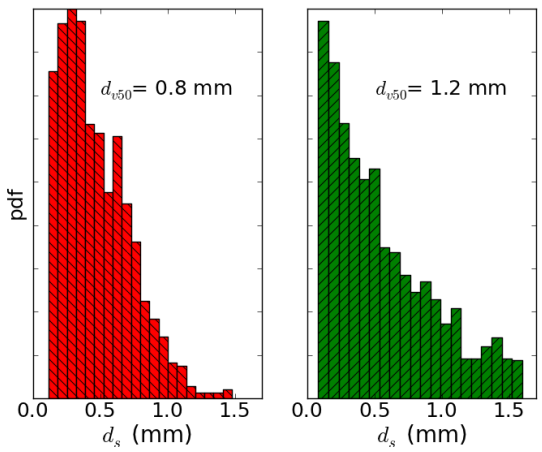

Figure 6. Diameter distribution for We = 810 including measured and simulated.

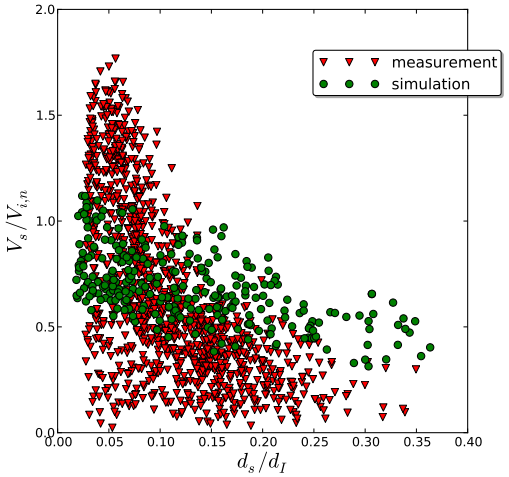

Figure 7. Comparisons of simulated secondary droplet velocity and diameter with experimentally measured values.